Ab initio calculation of phonons for bulk TiC and TiC(001)(1×1)

S. Bağcı,[1] T. Kamış,[1] H. M. Tütüncü,[1] and G. P. Srivastava[2]
[1]*Fen-Edebiyat Fakültesi, Fizik Bölümü, Sakarya Üniversitesi, 54187 Adapazarı, Turkey*
[2]*School of Physics, University of Exeter, Stocker Road, Exeter EX4 4QL, United Kingdom*
(Received 20 March 2009; revised manuscript received 10 June 2009; published 8 July 2009)

We present an *ab initio* pseudopotential study, within the local density functional approximation, of the structural and elastic properties of rock-salt TiC. The calculated structural and elastic properties of TiC are in good agreement with reported experimental values. Using the density-functional perturbation theory, the phonon spectrum and density of states are calculated. Good agreement has been found between the calculated and reported experimental dispersion curves. Following these bulk properties, we have made theoretical investigations of the atomic geometry and lattice dynamics of the TiC(001)(1×1) surface. The calculated surface structural parameters compare very well with available experimental values. Using our calculated surface phonon spectrum, we provide a detailed analysis of available experimental data from electron energy-loss spectroscopy.

DOI: 10.1103/PhysRevB.80.035405 PACS number(s): 63.20.dk, 68.35.Ja, 68.35.bd

I. INTRODUCTION

Transition-metal carbides have in general been the subject of intensive research over the past thirty years. There are several reasons for studying these materials. On the microscopic level, they are known to exist in the rock-salt structure and show a combination of three different types of bonding characteristics: metallic, ionic, and covalent.[1–6] With their covalent bonding, they exhibit extreme hardness and brightness[2,4] as diamond and other covalent solids. Other striking properties of these materials are their very high melting points as well as metallic conductivity,[7] comparable with those of pure transition metals. One such compound, TiC, is a highly stable field-electron emitter[8,9] which is needed in advanced lithography techniques for the production of integrated electronic circuits. Moreover, this material can be used as catalyst for surface chemical reactions.[10] Several experimental[11,12] and theoretical studies[13–18] have been done on the structural and elastic properties of TiC. Systematic theoretical efforts[19–21] have been made for phonons in TiC while an experimental study of the full phonon spectrum was presented by Pintschovius.[19]

In contrast to the wealth of theoretical work presented on the structural and elastic properties of bulk TiC, there has been limited experimental and theoretical work on its surfaces. On the experimental side, low-energy ion scattering (LEIS)[22] and low-energy electron diffraction (LEED)[23] experiments have been used to determine structural properties of its (001) surface. The phonon spectrum of this surface have been measured using electron energy-loss spectroscopy (EELS).[24] Theoretical studies have been made using a full-potential linear muffin tin orbital (LMTO),[25] tight-binding,[26] first-principles molecular dynamics (FPMD),[27] and density functional theory (DFT) calculations within the generalized gradient approximation (GGA)[28] and a 12-parameter shell model.[24]

In the present work we first aim to investigate the structural, elastic, and dynamical properties of rock-salt TiC by employing the plane-wave pseudopotential method, the density functional theory, and the linear response technique.[29] The calculated structural and elastic parameters are compared with available experimental and theoretical results. The second and main aim of the present work is to determine the structural and vibrational properties of the (001) surface of TiC using the same theoretical approach as used in bulk studies. The calculated surface atomic geometry is compared with available theoretical,[25–28] and experimental results[22,23] in detail. We also provide a detailed discussion of surface vibrations on the TiC(001) surface and compare our results with experimental data[24] and 12-parameter shell model calculations.[24]

II. THEORETICAL METHODS

Our calculations were performed in the framework of the density functional theory, within the local-density approximation (LDA) using the Ceperley-Alder correlation[30] as parametrized by Perdew and Zunger.[31] The electron-ion interactions were treated by using norm-conserving *ab initio* pseudopotentials.[32] A basis set containing all plane waves up to the cutoff energy of 60 Ry has been used. Since the crystal structure considered here is metallic, convergence is achieved using 75 special **k** points in the irreducible wedge of the Brillouin zone (BZ) of the rock-salt structure. Integration of functions in the momentum space up to the Fermi surface is done with a Gaussian smearing technique, with the smearing parameter of 0.02 Ry. The ground state properties of bulk TiC are determined by minimization of the total energy with respect to the unit-cell volume V. Then, the theoretical equilibrium lattice constant a, the static bulk modulus B, and the first-order pressure derivative of the bulk modulus B' have been obtained by fitting the calculated static total energies as a function of volume to the Murnaghan equation of state.[33]

The rock-salt structure has only three independent elastic constants, namely, C_{11}, C_{12}, and C_{44}. Thus, a set of three equations is needed to obtain these constants. C_{11}-C_{12} and C_{44} are calculated by volume-conserving tetragonal and monoclinic strains,[34,35] respectively. In order to obtain C_{11}

TABLE I. Lattice constant a, bulk modulus B, the pressure derivative of bulk modulus B′, and elastic constants (in unit of Mbar) for TiC are compared with other theoretical and experimental data.

	a (Å)	B (Mbar)	B′	C_{11}	C_{12}	C_{44}
TiC (present work)	4.26	2.765	3.90	5.88	1.25	1.79
Theory (LDA)[a]	4.27	2.770				
Theory (LDA)[b]	4.38	2.670				
Theory (LDA)[c]	4.25	2.700		6.06	1.06	2.30
Theory (GGA)[d]	4.35	2.730	4.30			
Theory (GGA)[e]	4.33	2.520				
Experimental[f]	4.33	2.400				
Experimental[g]				5.13	1.06	1.78

[a]Reference 17.
[b]Reference 15.
[c]Reference 13.
[d]Reference 16.
[e]Reference 18.
[f]Reference 11.
[g]Reference 12.

and C_{12} separately, the relationship between these elastic constants and bulk modulus

$$B = \frac{C_{11} + 2C_{12}}{3} \quad (1)$$

is also used. The elastic constants calculations require a very high degree of precision because the energy differences involved are of the order less than 1 mRy. Ensuring the required accuracy in total energy results requires the use of a fine **k**-point mesh. We thus calculated the elastic constants by using a $24 \times 24 \times 24$ Monkhorst-Pack **k** mesh.[36]

The lattice dynamics of bulk TiC was studied within the framework of the self-consistent density-functional perturbation theory.[29] Within this scheme, second-order derivatives of the total energy were calculated to obtain the dynamical matrix. A static linear response of the valence electrons was considered in terms of the variation in the external potential corresponding to periodic displacements of the atoms in the unit cell. The screening of the electronic system in response to the displacement of the atoms was taken into account in a self-consistent manner. A $12 \times 12 \times 12$ **k** mesh was found to yield phonon frequencies converged to within 0.05 THz, and this was used in our calculations. A $4 \times 4 \times 4$ **q** mesh in the first BZ was used in the interpolation of the force constants for the phonon dispersion curve calculations. Phonon density of states calculations were made by using the tetrahedron method.

For surface calculations, we used an artificially periodic slab geometry along the surface normal direction of [001]. In the present case, a supercell is considered to contain thirteen layers of TiC and a vacuum region equivalent to five layers of TiC. The energy cutoff was the same as for the bulk calculations, but the surface BZ was sampled by six special **k** points. All atoms were allowed to relax into their minimum energy configuration, except for the atoms in the middle of slab which are kept frozen. The relaxation was carried out using a conjugate gradient algorithm, utilizing the forces obtained from the solution of the Kohn-Sham equation at each iterative step. The equilibrium atomic positions were obtained with numerical uncertainty of less than 0.01 Å, with forces on all atoms becoming smaller than 0.1 mRy/a.u. The phonon spectrum of the TiC(001) surface was also obtained by applying the density-functional perturbation scheme, based upon the pseudopotential method used for the structural studies. In order to generate the force-constant matrices for this surface, and to carry out the inverse Fourier transformation, we used **q** points on a $4 \times 4 \times 1$ mesh. All calculations were carried out by using the code PWSCF (Plane-Wave Self-Consistent Field).[29]

III. RESULTS

A. Bulk properties

Before discussing surface results, it is very useful to analyze the quality of pseudopotentials with TiC bulk calculations, comparing the key structural parameters with previous theoretical and experimental results. The bulk static properties of this material were obtained using the calculations of the total energy as a function of lattice constant. These bulk properties from the total energy calculations are summarized in Table I with available experimental[11,12] and theoretical[13,15–18] results. In general, the agreement between experiment and the present calculations is good. The calculated lattice constant is only 2% smaller than the experimental value of 4.33 Å, which is a typical consequence of the LDA calculations. However, the static bulk modulus of this material is overestimated by about 13% than its experimental value. On the other hand, the presently determined value of bulk modulus is in good agreement with the previous LDA results.[13,15,17] One should also notice that the experimental value of the bulk modulus is somehow uncertain due to the difficulty of growing good quality single crystal of TiC.

It is well known that the elastic properties define the properties of a material that undergoes stress, deforms, and then

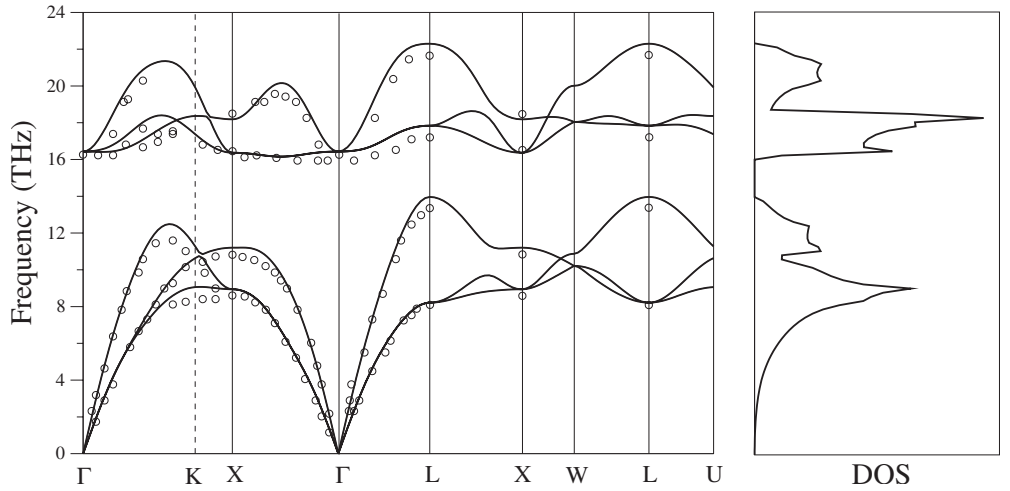

FIG. 1. Theoretical phonon dispersion curves and density of states for TiC. Experimental data (open circles) are taken from Ref. 19.

recovers and returns to its original shape after stress ceases. In fact, there are three elastic constants for the rock-salt structure, denoted as C_{11}, C_{12}, and C_{44}. These three independent elastic constants are estimated by calculating the stress tensors on applying strains to an equilibrium structure. In Table I, we show our results regarding the elastic constants for TiC in the rock-salt structure at zero pressure. All elastic constants in this table are positive and satisfy the generalized criteria for mechanically stable crystals: $(C_{11}-C_{12})>0$; $C_{11}+2C_{12}>0$; $C_{11}>0$; and $C_{44}>0$. For comparison, available experimental[12] and theoretical[13] results are also listed in Table I. We see that the calculated elastic constants are in reasonably good agreement with the existing experimental data[12] within the experimental uncertainties. The deviations vary between 0.6% and 18%, the best agreement being found for C_{44}.

The results of the bulk phonon-dispersion curves are displayed in Fig. 1, along several high-symmetry lines, together with the corresponding phonon density of states (DOS). The experimental data from Ref. 19 is shown by open circles in this figure. The overall agreement with the experimental data is fairly good. Since the unit cell contains two atoms, there are six vibrational phonon modes for any chosen **q** point. For wave vectors along [100] and [111], the transverse modes are doubly degenerate. Therefore, there are only four distinct values of frequencies in these directions. In the [110] direction, the transverse modes are not degenerate and thus there are six distinct frequencies in this direction. Due to the large mass difference between Ti and C atoms, the optical phonon branches are well separated from the acoustic branches. The longitudinal optical (LO) frequencies increase rather rapidly with increasing **q**. However, transverse optical (TO) branches show reduced amounts of dispersion along the [110] and [111] directions, and nearly no dispersion along the [100] direction. The flatness of TO branch along [100] gives rise to a peak in the DOS at 16.5 THz. The peak at 18.2 THz is also due to the TO branches while the peak centered at around 20.6 THz comes from the LO branch. The computed transverse and longitudinal acoustic (TA and LA) branches behave normally in the long wave limit, with steep slopes. We have observed that the lower TA branch is nearly flat near the Brillouin zone boundaries *X* and *L*. This flatness leads to a clear peak at 9.0 THz in the DOS, while the LA phonon branch creates a peak centered at around 11.7 THz.

In order to test our LDA results for phonons in TiC, we also used a first-principles pseudopotential method based on a GGA of the density functional theory. We have used the ultrasoft pseudopotentials.[37] The electronic wave functions are expanded in plane waves up to a maximum cutoff energy of 50 Ry. Our numerical results are obtained using the GGA functional by Perdew-Burke-Ernzerhof.[38] Our GGA phonon calculations have been made at the Γ, *X*, and *L* symmetry points. Comparison of LDA and GGA phonon results for TiC has been made in Table II. It should be pointed out that there is no systematic increase or decrease in phonon frequencies due to the inclusion of the GGA. However, results from both methods are in good agreement between each other. The LDA phonon results presented in Table II do not change more than 7% when GGA method is employed. This change is within typical experimental error margin. Thus, we can say that LDA results are of as good a quality as the GGA results are.

TABLE II. Comparison of LDA and GGA phonon results (in THz) for TiC at the Γ, *X*, and *L* symmetry points. Experimental results are also presented.

Symmetry point (Method)	TA	LA	TO	LO
Γ (LDA)			16.43	16.43
Γ (GGA)			15.21	15.21
Γ (EXP)[a]			16.08	16.08
X (LDA)	8.94	11.20	16.38	18.18
X (GGA)	9.19	11.24	15.29	17.49
X (EXP)[a]	8.69	10.72	16.38	18.55
L (LDA)	8.21	13.96	17.84	22.29
L (GGA)	8.36	13.85	16.88	21.48
L (EXP)[a]	7.97	13.13	17.10	21.45

[a]Reference 19.

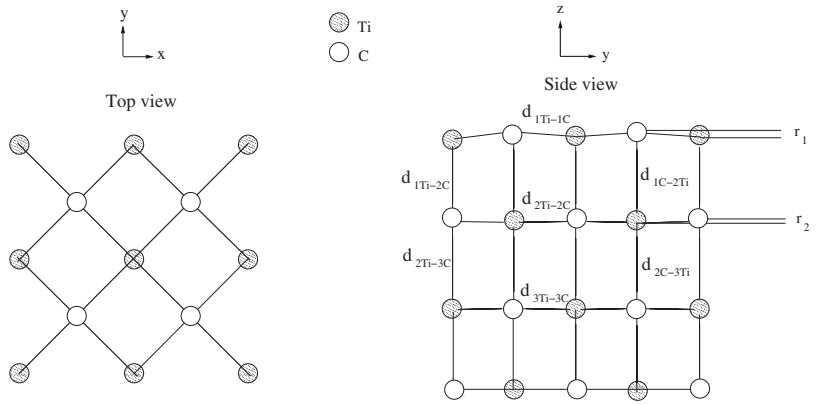

FIG. 2. Schematic illustration of relaxed side and top views of the TiC(001)(1×1) surface. The vertical buckling of top two layers (r_1 and r_2) and the bond lengths ($d_{Ti\text{-}C}$) are also shown in the side view of the surface.

B. Surface properties

1. Atomic geometry

Before discussing our results for phonons on the TiC(001) surface, we will briefly address the results for atomic geometry. The cleaved (001) surface of rock-salt TiC retains the primitive (1×1) periodicity, but its surface presents a very well-known pattern of relaxation. Each atom is situated at the center of a square net of atoms of the other type. At the surface and subsurface layers, Ti atoms move away from the bulk, while the C atoms move into the bulk. Schematic side and top views of the relaxed surface geometry of the TiC(001) surface are illustrated in Fig. 2. The structural parameters indicated in Fig. 2 are also listed in Table III. These parameters are in good agreement with the experimental LEED[23] study and previous theoretical calculations.[27,28] In particular, the calculated values of the vertical buckling of the top two layers (r_1 and r_2) are found to be 0.12 and 0.04 Å, respectively. These values compare very well with their corresponding experimental values of 0.14 and 0.03 Å (Ref. 23) within the experimental uncertainties. Our calculated r_1 and r_2 values are also in good agreement with the recent GGA values[28] of 0.11 and 0.03 Å. For the relaxed surface, bond lengths are found to deviate significantly. In particular, the bond length between the surface layer Ti and the subsurface layer C (d_{1Ti-2C}) is found to be 2.031 Å, which is 5% smaller than the calculated bulk bond length value of 2.13 Å. The experimental value of d_{1Ti-2C} has been reported to be 2.14 Å in the LEED measurement by Tagawa *et al.*[23] The other bond lengths (d_{1C-2Ti}, d_{2Ti-3C}, and d_{2C-3Ti}) are found to be 2.188, 2.077, and 2.142 Å, respectively. These values are in reasonable agreement with the corresponding experimental values of 2.25, 2.19, and 2.15 Å.[23]

2. Phonon spectrum and density of states

As noted earlier, there is a large gap between the bulk acoustic and optical phonon branches due to the mass difference between Ti and C atoms. Any solutions found in this gap region will be truly localized surface states. In addition to this gap region, there are a few stomach gaps in the projected bulk phonon band structure. The first of these lies in the bulk acoustic phonon region. This gap is due to the energy difference between LA and TA phonon modes in the bulk phonon spectrum of TiC. Other two gaps come from the energy difference between LO and TO phonon energies. No bulk phonon states can be found in these gap regions.

The calculated phonon spectrum for the TiC(001) surface is shown in Fig. 3. The calculated results are shown by thick lines while the projected bulk TiC phonon energies are shown by the shaded regions. The dashed curves in this figure indicate surface phonon results with the ideally terminated surface geometry. Open squares illustrate the EELS data from the experimental work of Oshima *et al.*[24] The calculated results are in good agreement with the experimental data along the all symmetry directions. We find that several surface localized phonon states appear throughout the surface Brillouin zone (SBZ) in the acoustic-optical gap range.

TABLE III. Vertical buckling of top two layers (r_1 and r_2) and the calculated bond lengths ($d_{Ti\text{-}C}$), compared with previous experimental and theoretical results. Units: Å.

Source	r_1	r_2	d_{1Ti-1C}	d_{2Ti-2C}	d_{3Ti-3C}	d_{1Ti-2C}	d_{1C-2Ti}	d_{2Ti-3C}	d_{2C-3Ti}
This work	0.120	0.040	2.124	2.122	2.122	2.031	2.188	2.077	2.142
LEED[a]	0.14	0.03				2.14	2.25	2.19	2.15
GGA[b]	0.11	0.03							
FPMD[c]	0.14								

[a]Reference 23.
[b]Reference 28.
[c]Reference 27.

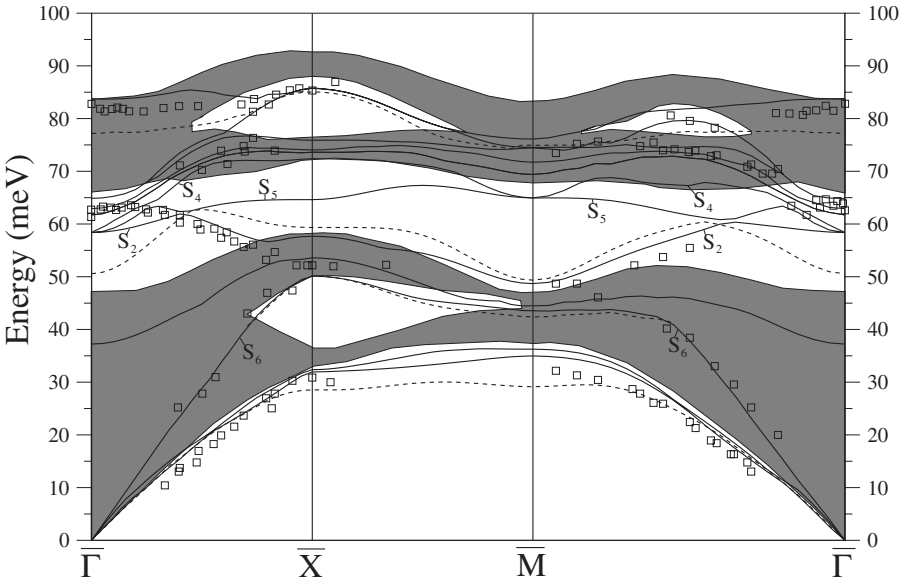

FIG. 3. Theoretical surface phonon dispersion curves of the relaxed (solid curves) and unrelaxed (dotted curves) TiC(001)(1×1) surface. Experimental results[24] are depicted by open squares.

Three of these, labeled S_2, S_4, and S_5, are degenerate at the Γ point. Good agreement has been observed between our calculated and experimental results[24] for the S_2 phonon branch along the $\bar{\Gamma}$-$\bar{X}$ and $\bar{\Gamma}$-$\bar{M}$ directions. The branch S_4 is dispersive up to the middle of $\bar{\Gamma}$-$\bar{X}$ direction. Close to the zone boundary point $\bar{X}$, this branch is nearly flat and it turns into a delocalized surface phonon mode. The branch lying between S_2 and S_4 has been labeled S_5 in the literature. As can be seen from Fig. 3, this phonon branch is less dispersive than the S_2 and S_4 branches. The phonon branches in the LO and TO gap regions are also in good agreement with experimental measurements.[24] In addition to these branches, any solutions found above and below the bulk phonon regions will be states truly localized at the surface. However, we have not found any localized phonon branch above the bulk phonon spectrum. This observation is in good agreement with experimental results.[24] Our highest surface optical-phonon branch lies 3 meV below the projected bulk continuum. The picture for the lowest surface acoustic branch is different. This branch, known as the Rayleigh wave branch, is found to fall below the bulk-acoustic continuum and becomes truly localized close the zone edges and along the $\bar{X}$-$\bar{M}$ direction.

We have made a few observations regarding the importance of surface relaxation on the energy location of phonon modes. First, surface relaxation shifts the highest surface optical state upward in energy by up to 5 meV at the zone center. Second, the lowest gap phonon mode for the unrelaxed geometry lies 8 meV below the corresponding relaxed phonon mode at the zone center. Moreover, the agreement between the unrelaxed-gap phonon modes and experimental values is not as good as the corresponding agreement between the relaxed-gap phonon modes and experimental values.[24] Finally, the energy of the Rayleigh mode at the zone center shifts upward by about 4 meV due to surface relaxation.

In Fig. 4(a), we have plotted the phonon DOS for the TiC(001), surface (solid curves), and bulk TiC (dashed

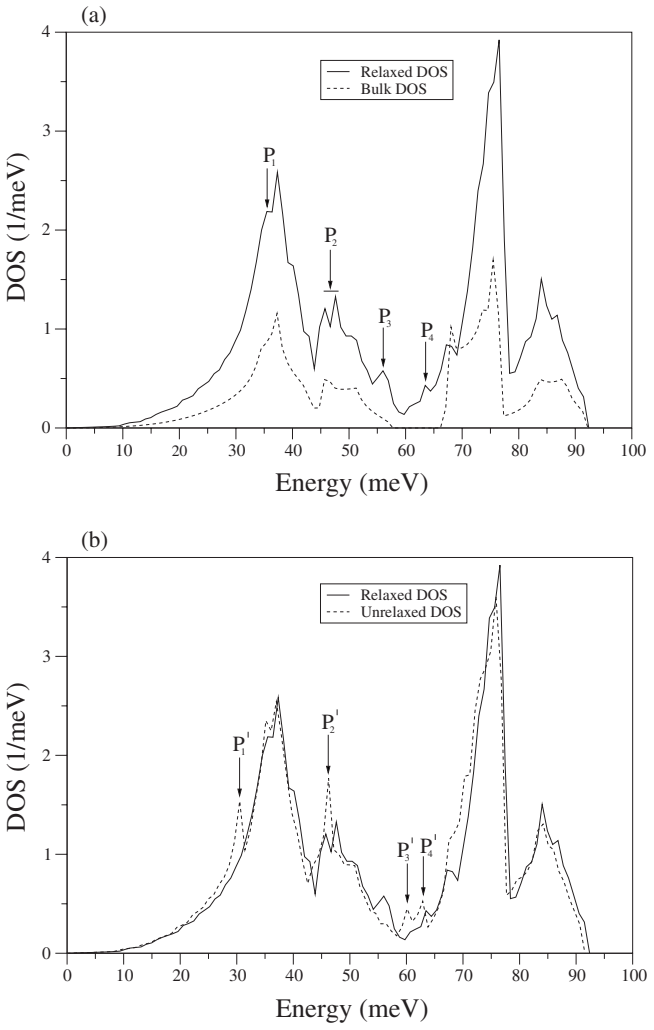

FIG. 4. Theoretical results for surface-phonon density of states of the TiC(001)(1×1) surface (a) relaxed and bulk DOS, (b) relaxed and unrelaxed DOS.

TABLE IV. Polarization characters of the zone-center phonon frequencies (in meV) and comparison with a previous shell model calculation.

	SH modes			SP modes			
This work	58.40	63.51	58.40	58.40	62.90	64.60	83.80
Shell Model[a]	64.30		64.30	64.30			81.00
Classification	S_5		S_4	S_2			S_2'

[a]Reference 24.

curves). Some of the clearly identified peaks due to surface phonon states are labeled P_1-P_4. The peak P_1 (at around 35 meV) is due the Rayleigh wave branch along the $\bar{X}$-$\bar{M}$ direction. The peak P_2 is characterized by localized gap phonon modes along the same symmetry direction. We have observed two clear peaks at energies 56 and 64 meV which are due to localized-gap phonon modes in the acoustic-optical gap region. In order to show the overall effect of surface relaxation on vibrations clearly, the phonon density of states for relaxed and unrelaxed geometries are shown in Fig. 4(b). The surface phonon peaks obtained for the relaxed geometry are also found for the unrelaxed-surface geometry. These peaks are labeled P_1' to P_4' have same character with their corresponding peaks in Fig. 4(a). The energy difference between these peaks can be related to the relaxation of surface.

3. Polarization and localization of surface phonon modes

In this paper, phonon dispersion curves for the TiC(001) surface are plotted corresponding to vibrations of atoms in the top two layers. Since the top two layers have four atoms in the unit cell, it is expected that vibrations of these atoms would result in 12 surface phonon modes. We will discuss polarization characteristics of these phonon modes at the symmetry points $\bar{\Gamma}$, $\bar{X}$, and $\bar{M}$. Before making this discussion, it is important to note that when the wave vector is along the $\bar{\Gamma}$-$\bar{X}$ and $\bar{\Gamma}$-$\bar{M}$ axes, there is a mirror reflection symmetry about the plane which contains the surface normal and the wave vector. Thus, the vibration is separated into a saggital plane (SP) mode which oscillates in the plane and a shear horizontal (SH) mode whose eigenvector is vertical to the plane. Only the SP modes are observable by the EELS experimental technique in Ref. 24.

The calculated zone-center surface phonon frequencies for TiC(001) and their comparison with previous shell model calculations[24] are given in Table IV. The surface-phonon modes listed in this table are named (S_2, S_4, and S_5) in a way similar to Chen's classification.[39] The phonon branches S_2, S_4, and S_5 are degenerate at zone center with energy 58.40 meV. The energy of this zone-center phonon mode has been reported at 64.0 meV in the previous shell model calculation.[24] We believe that this energy difference is largely due to a proper treatment in the present work of interatomic force constants and effective charges at the surface layer. Away from the zone center, the three branches split off. This can be seen clearly along $\bar{\Gamma}$-$\bar{X}$ in Fig. 3. The phonon modes at 62.90 and 64.60 meV have SP character, while the phonon at 63.51 meV has SH character. It is important to note that the shear phonon mode at 63.51 meV cannot be observed experimentally due to its vibrational pattern. These phonon modes are all localized gap phonon modes in the acoustic-optical gap region. The highest gap phonon mode at 64.60 meV is mainly localized on the first layer C atoms, while other gap phonon modes come from the vibrations of second layer C atoms due to large mass difference between Ti and C atoms. In agreement with previous shell model calculation, the highest surface optical phonon mode at 83.80 meV has SP character. This phonon mode is dominated by atomic vibrations of the second-layer C atoms in the surface normal direction. This phonon mode has been labeled S_2' in the literature. The energy of this phonon mode is in excellent agreement with the EELS[24] results at around 85.0 meV.

Along the $\bar{\Gamma}$-$\bar{X}$ direction, we have identified three surface acoustic branches. Two of these fall below the bulk acoustic continuum and become truly localized-phonon modes away from zone center. The energy difference between these branches is very small (less than 1 meV). The third branch becomes separated from the other branches with increasing wave vector. Close to the zone-edge $\bar{X}$ point, this branch falls into a stomach-gap region. The lowest acoustic branch is totally polarized with SH character while other acoustic branches have SP character. These characters are slightly different from their corresponding characters determined from the shell model calculations. Oshima *et al.*[24] have observed the SP and SH characters for the first and second acoustic branches, respectively. Noting that the experimental measurements and theoretical estimates have error margins of 1 meV, this character change is quite acceptable due to very small energy difference between these branches. At the zone edge $\bar{X}$, the energies of these branches are found to be 31.95, 32.69, and 50.16 meV. We present displacement patterns of these phonon modes in Fig. 5. The lowest frequency is a transverse acoustic phonon mode due to the motion of the first-layer Ti and second-layer C atoms in the [010] direction. The second acoustic frequency also includes large atomic vibration from first-layer Ti and second-layer C atoms in the surface normal direction, while the second-layer Ti atom move in the wave vector direction with smaller amplitudes. As a result of this vibrational picture, this phonon mode may be described as a quasitransverse acoustic mode. The third surface acoustic frequency has an energy of 50.16 meV and is characterized by large atomic vibrations of surface-layer Ti atoms in the wave vector direction. For this phonon mode, first-layer C atoms vibrate in the surface normal direction but with smaller amplitudes than vibrational amplitudes of first-layer Ti atoms. In the literature, this phonon mode is known

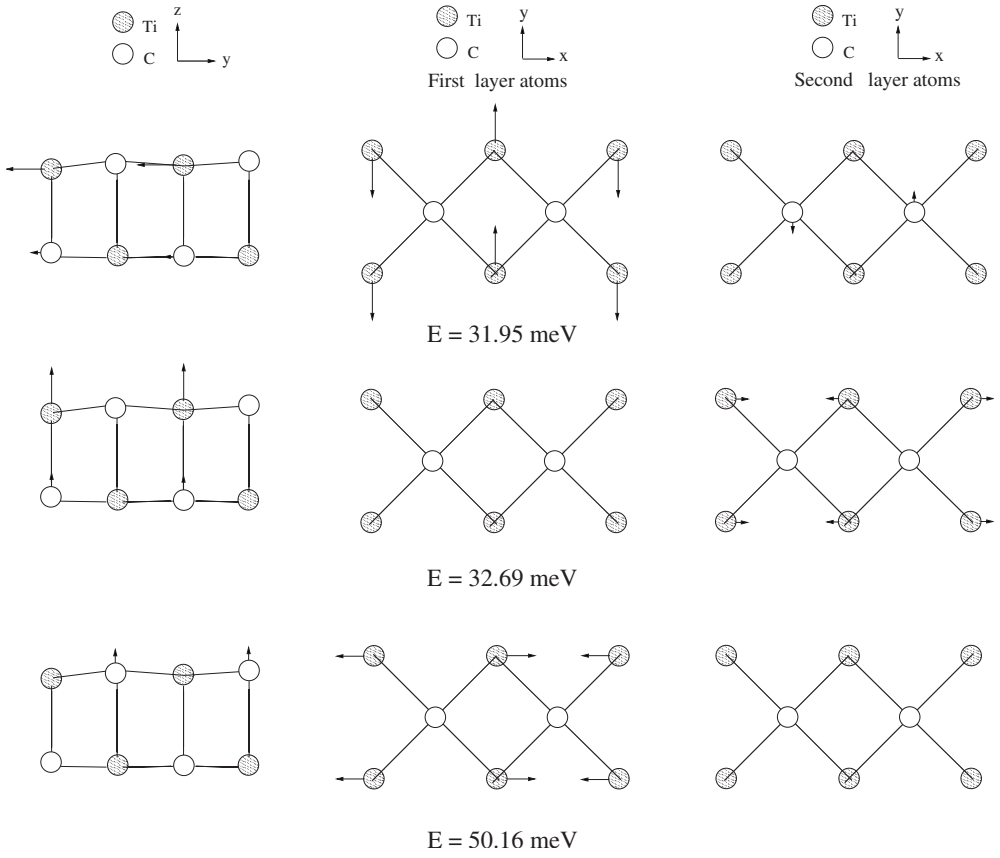

FIG. 5. Atomic displacement patterns for surface acoustic phonon modes at the $\bar{X}$ point.

as a quasilongitudinal acoustic mode because of its vibrational pattern. The branch S_5 has SH character due to the vibrations of surface-layer C atoms in the [010] direction. The other atoms are nearly at rest for this phonon mode. In the literature, this frequency is known as the Lucas mode. We additionally report that this phonon mode is purely transverse optical due to its vibrational picture. The S_2 and S_4 modes have SP character which are in agreement with the shell model calculations of Oshima *et al.*[24] Finally, the energy of highest surface optical phonon mode is found at 85.83 meV, which is in good agreement with its experimental value of 85.0 meV. This phonon mode includes large atomic vibrations from the surface-layer C atoms in the wave vector direction while the second-layer C atoms move in the surface normal direction with smaller amplitudes. As a results of this picture, this mode can be labeled as a quasilongitudinal optic mode.

Along the $\bar{\Gamma}$-$\bar{M}$ direction, the vibrations of the surface-layer Ti atoms increase with the wave vector for the lowest and second acoustic phonon modes, thus turning into truly localized phonon modes at the zone-edge $\bar{M}$ point. In agreement with the previous shell model calculations,[24] these acoustic phonon modes have SP and SH characters, respectively. The dispersion of the third acoustic-phonon mode agrees very well with the experimental data along this symmetry direction. We have observed SP character for this phonon mode, in agreement with the shell model calculation of Oshima *et al.*[24] Due to atomic displacement patterns of these acoustic branches, first two of these are TA phonon modes while third one is LA phonon mode. Similar observation has been also made at the $\bar{X}$ point. The energies and polarization characters of these phonon modes are presented and compared with previous theoretical calculations[24] in Table V. At the zone-edge $\bar{M}$ point, S_4 (SP character) and S_5 (SH character) branches become degenerate at 64.36 meV which can be seen in Table V. The S_2 phonon branch shows similar dispersion to the corresponding phonon mode along the $\bar{\Gamma}$-$\bar{X}$

TABLE V. Frequencies (in meV) and polarization character of phonon modes at the $\bar{M}$ point and comparison with a previous shell model calculation.

	SH modes			SP modes			
This work	36.36	65.0	34.73	43.55	48.91	65.0	76.13
Shell Model[a]	33.57	64.6	30.35	37.86	48.57	64.6	75.0
Classification	S_1'	S_5	S_1	S_6	S_2	S_4	

[a]Reference 24.

direction. Moreover, this phonon branch has vibrational pattern similar to its counterpart along the $\bar{\Gamma}$-$\bar{X}$ direction. The highest surface optical-phonon mode in the $\bar{\Gamma}$-$\bar{M}$ direction starts at $\bar{\Gamma}$ as the vibrations of the second-layer C atoms in the surface normal direction and this SP character continues up to the most part of this symmetry direction. However, approaching the zone boundary it switches his character to SH. At the $\bar{M}$ point, we have found that this phonon mode is characterized by atomic vibrations of the second-layer atoms in the wave vector direction. Due to its vibrational character, this phonon mode is purely LO, with SH polarization character.

IV. SUMMARY

In this paper, we have presented the structural, elastic and vibrational properties of rock-salt TiC by employing a first-principles scheme based on the application of the plane-wave pseudopotential method, density functional theory, and a linear response technique. The calculated static properties, viz., equilibrium lattice constant a, bulk modulus B, and pressure derivative of bulk modulus B′ are in agreement with previous theoretical and available experimental results. In order to calculate elastic constants for rock-salt TiC, we have applied tetragonal and monoclinic strains. Our calculated C_{44} value is in excellent agreement with its experimental value. In addition to this agreement, the calculated phonon dispersion curves for rock-salt TiC fit very well with experimental data.

We have also performed *ab initio* pseudopotential calculations for structural properties of the TiC(001)(1×1) surface. The calculated structural parameters and bond lengths compare very well with existing experimental data. The presently obtained relaxed atomic geometry is used for the calculations of the surface phonon modes on this surface using the linear response approach based on an *ab initio* pseudopotential method and the local-density functional perturbation scheme. The calculated phonon dispersion curves are in good agreement with the experimental data. We have provided a more detailed account of surface vibrations than is currently available from experiments or other theoretical calculations. We have also examined the effect of surface relaxation on surface phonon modes. In particular, we have noted that the highest surface optical phonon branch and the lowest acoustic-optical gap branch are very sensitive to surface relaxation. We have provided a detailed account of the polarization of atomic vibrations along the $\bar{\Gamma}$-$\bar{X}$ and $\bar{\Gamma}$-$\bar{M}$ directions. Moreover, the polarization characteristics of various zone-center and zone-edge phonon modes have been presented and discussed in detail.

ACKNOWLEDGMENTS

This work was supported by the Scientific and Technical Research Council of Turkey (TUBİTAK).

[1] M. Gupta and A. J. Freeman, Phys. Rev. B **14**, 5205 (1976).
[2] K. Schwarz, J. Phys. C **10**, 195 (1977).
[3] B. M. Klein, D. A. Papaconstantopoulos, and L. L. Boyer, Phys. Rev. B **22**, 1946 (1980).
[4] P. Blaha and K. Schwarz, Int. J. Quantum Chem. **23**, 1535 (1983).
[5] K. Schwarz, Crit. Rev. Solid State Mater. Sci. **13**, 211 (1987).
[6] A. Fernández Guillermet, J. Häglund, and G. Grimvall, Phys. Rev. B **45**, 11557 (1992).
[7] P. A. P. Lindberg, L. I. Johansson, J. B. Lindström, P. E. S. Persson, D. S. L. Law, and A. N. Christensen, Phys. Rev. B **36**, 6343 (1987).
[8] C. Oshima, T. Tanaka, M. Aono, R. Nishitani, S. Kawai, and F. Yajima, Appl. Phys. Lett. **35**, 822 (1979).
[9] I. Kojima, E. Miyazaki, Y. Inoue, and I. Yasumori, J. Catal. **59**, 472 (1979).
[10] S. Zaima, C. Oshima, S. Otani, M. Aono, H. Adachi, and Y. Shibata, in *Proceedings of the 28th International Field Emission Symposium, Beaverton, 1981*, edited by L. Swanson and A. Bell, p. 156.
[11] J. E. Holliday, in *Advance in X-ray Analysis*, edited by B. L. Henke, J. B. Newkirt, and G. R. Mallet (Plenum Press, New York, 1970), Vol. 13, p. 136.
[12] M. M. Choy, W. R. Cook, R. F. S. Hearmon, H. Jaffe, J. Jerphagnon, S. K. Kurtz, S. T. Liu, and D. F. Nelson, in *Elastic, Piezoelectric, Pryoelectric, Piezooptic, Electrooptic Constants, and Nonlinear Dielectric Susceptibilities of Crystals*, edited by K.-H. Hellwege and A. M. Hellwege, Landolt-Börnstein, Numerical Data and Functional Relationship in Science and Technology, Vol. 11 (Springer, Berlin, 1979).
[13] R. Ahuja, O. Eriksson, J. M. Wills, and B. Johansson, Phys. Rev. B **53**, 3072 (1996).
[14] S.-H. Jhi and J. Ihm, Phys. Rev. B **56**, 13826 (1997).
[15] J. C. Grossman, A. Mizel, M. Cote, M. L. Cohen, and S. G. Louie, Phys. Rev. B **60**, 6343 (1999).
[16] S. Mecabih, N. Amrane, Z. Nabi, B. Abbar, and H. Aourag, Physica A **285**, 392 (2000).
[17] Z. Dridi, B. Bouhafs, P. Ruterana, and H. Aourag, J. Phys.: Condens. Matter **14**, 10237 (2002).
[18] L. Liu, S. Wang, and H. Ye, J. Mater. Sci. Technol. **19**, 540 (2003).
[19] L. Pintschovius, W. Reichardt, and B. Scheerer, J. Phys. C **11**, 1557 (1978).
[20] P. T. Jochym, K. Parlinski, and M. Sternik, Eur. Phys. J. B **10**, 9 (1999).
[21] E. I. Isaev, S. I. Simak, I. A. Abrikosov, R. Ahuja, Yu. Kh. Vekilov, M. I. Katsnelson, A. I. Lichtenstein, and B. Johansson, J. Appl. Phys. **101**, 123519 (2007).
[22] M. Aono, Y. Hou, R. Souda, C. Oshima, S. Otani, and Y. Ishizawa, Phys. Rev. Lett. **50**, 1293 (1983).
[23] M. Tagawa, M. Okuzawa, T. Kawasaki, C. Oshima, S. Otani, and A. Nagashima, Phys. Rev. B **63**, 073407 (2001).
[24] C. Oshima, T. Aizawa, M. Wuttig, R. Souda, S. Otani, Y. Ishizawa, H. Ishida, and K. Terakura, Phys. Rev. B **36**, 7510

(1987).
[25] D. L. Price, J. M. Wills, and B. R. Cooper, Phys. Rev. Lett. **77**, 3375 (1996).
[26] K. E. Tan, A. P. Horsfield, D. N. Manh, D. G. Pettifor, and A. P. Sutton, Phys. Rev. Lett. **76**, 90 (1996).
[27] K. Kobayashi, Jpn. J. Appl. Phys., Part 1 **39**, 4311 (2000).
[28] F. Vines, C. Sousa, P. Liu, J. A. Rodriguez, and F. Illas, J. Chem. Phys. **122**, 174709 (2005).
[29] S. Baroni, S. de Gironcoli, A. Dal Corso, and P. Giannozzi, Rev. Mod. Phys. **73**, 515 (2001).
[30] D. M. Ceperley and B. J. Alder, Phys. Rev. Lett. **45**, 566 (1980).
[31] J. P. Perdew and A. Zunger, Phys. Rev. B **23**, 5048 (1981).
[32] R. Stumpf, X. Gonze, and M. Scheffer, *A List of Separable, Norm-Conserving, Ab-initio Pseudopotentials* (Fritz-Haber-Institut, Berlin, 1990).
[33] F. D. Murnaghan, Proc. Natl. Acad. Sci. U.S.A. **50**, 697 (1944).
[34] M. J. Mehl, J. E. Osburn, D. A. Papaconstantopoulos, and B. M. Klein, Phys. Rev. B **41**, 10311 (1990).
[35] H. M. Tütüncü, S. Bağcı, and G. P. Srivastava, J. Phys.: Condens. Matter **19**, 156207 (2007).
[36] H. J. Monkhorst and J. D. Pack, Phys. Rev. B **13**, 5188 (1976).
[37] D. Vanderbilt, Phys. Rev. B **41**, 7892 (1990).
[38] J. P. Perdew, K. Burke, and M. Ernzerhof, Phys. Rev. Lett. **77**, 3865 (1996).
[39] T. Chen, G. P. Alldrege, F. W. deWette, and R. E. Allen, Phys. Rev. Lett. **26**, 1543 (1971).